An Experimental Study on Circulating Flow Around a
Submerged Horizontal Plate
잠재 평판 주변에서 발생하는 순환류에 대한 실험적 연구

Lee, Jung Lyul* and Han, Sang Woo**
이정렬* · 한상우**

Abstract □ This paper describes results of an experimental study to examine the effect of a submerged horizontal breakwater to sea water exchange. Flow measurements were taken by using a PIV(Particle Image Velocimetry) system, and mean currents and wave ellipses extracted through the harmonic analysis are presented. As results, the rates of circulating flow were closely connected with the volume flux of incident waves and the counter-rotating vortex pair was observed at the onshore side of a plate. The dye study showed that incoming sea water and polluted water body mixed up significantly due to turbulent motions induced by a jet-like flow.

Keywords : PIV, Plate-Type Breakwater, Sea Water Exchange, Circulating Flow, Vortex Pair, Wave Ellipse

要 旨 : 잠재된 평판 방파제가 해수 교환에 미치는 영향을 실험적으로 조사하였고 그 결과를 제시한다. 흐름은 PIV 시스템으로 관측되었으며 조회분석으로부터 분리된 평균 흐름과 파랑 타원이 각각 제시된다. 실험결과, 순환 유량은 입사파의 체적플럭스와 밀접한 관계가 있으며 쌍와류가 평판 후면에서 관측되었다. 염료추적에 의하면 평판위에서 발생된 제트류로 인한 난류의 영향으로 유입되는 해수와 항내 오염물질이 상당히 잘 섞이고 있음을 보여주고 있다.

핵심용어 : PIV, 평판제, 해수교환, 순환류, 쌍와류, 파랑 타원

1. INTRODUCTION

The most serious problems of marine pollution are encountered in industrialized and urbanized estuaries. Historically, most port grew up on estuaries and became center of population and industry. The urban and indus-trial wastes were often discharged directly into the port. With the growth of population and industry, therefore, the major industrial ports become foul, stinking, and lifeless. In ports, ships come and go carrying many toxic sub-stances in the course of trade: oil, liquefied natural gas, pesticides, industrial chemicals, and so on. Shipwrecks and other accidents may release these substances. Most tanker accidents occur near the port where the density of shipping is high and if the substances are released, coastal pollution almost invariably results. In the course of routine operations, ships discharge oily ballast water and bilge water and cargo tank washings. Therefore, ports always face environmental problems resulting in deleterious effects such as hazards to human health, hindrance of marine activities including fishing, impairment of the water quality for the use of seawater, and reduction of amenities.

The conventional surface-piercing breakwaters have been used in many years as a method of port protection from wave impacts, but they often cause the environmental problem. Therefore, persistent efforts have been devoted to developing efficient and economical breakwaters to improve water quality. There are three types of breakwaters to permit water exchange; bottom-seated submerged

*Associate Professor (Department of Civil and Environmental Engineering, Sungkyunkwan University. Suwon 440-746, Korea)
**Graduate Student (Department of Civil and Environmental Engineering, Sungkyunkwan University. Suwon 440-746, Korea)

breakwater, non-bottom-seated and non-overtopped break-water, and submerged plate breakwater. In this study, a submerged horizontal plate has been examined through laboratory experiments as a simple type of breakwater which controls the wave invasion and which permits the flushing. Since a plate breakwater has a shortcoming in wave reduction anyhow when compared with non-overtopped gravity structures, it is recommended that the plate breakwater should be employed in a corner portion of the conventional breakwater. Several useful studies for the reduction of wave energy transmission passing over it have been accumulated (Ayoyama et al., 1988; Yu et al., 1991), but less interest was given to flow characteristics around a submerged plate. Most recently, Murakami et al. (1994) investigated the characteristics of the temporal and spatial wave-induced flow and turbulence around a submerged sloping plate and discussed on the basis of the results of the water particle velocity measured by the Laser Doppler Velocimeter. Iwata et al. (1996) numerically simulated the strong return flow below the submerged structure. The flow structure is similar to that in surf zone because in both cases the return flows are generated to compensate the onshore volume transport within a surface layer under wave breaking.

In this study, a Particle Image Velocimetry (PIV) system is used to identify the characteristics and quantity of flow formed around a plate. PIV has been used extensively since the mid-1980's beause it offers many advantages over other conventional velocimetries, such as laser Doppler velocimetry and hot-wire anemometry. PIV (Adrian, 1991) is a superior flow visualization technique for providing an instantaneous, non-intrusive insight into velocity field distributions with qualitative and quantitative information.

An introduction of PIV to the process in a coastal engineering context was given by Greated et al. (1992). Since then, this technique has been widely used for examining internal characteristics of wave motions, but, in Korea, PIV is still accepted as a new technique in the field of coastal engineering as well as hydraulics engineering. Quinn et al. (1993) gave an account of the errors inherent in the technique and used it as an example for the measurement of waves breaking on a 1:30 plane sloping beach. Petti et al. (1994) utilized PIV techniques to display the vortex behaviors around a submerged breakwater.

Their study examined the velocity fields of waves breaking over submerged breakwaters, paying particular attention to the formation of large-scale vortices formed by the breaking waves. More recently, Emarat et al. (2000) studied the mechanics of a plunging breaker using PIV and Yamada and Takikawa (2000) improved a PIV system to satisfy the mass conservation law.

The PIV experimental method consists of seeding the flow with small particle tracers exposed with a thin light sheet which is usually provided by a laser and acquiring the particle images resulting from the successive exposures recorded with an image sensor. Frequency domain techniques are used to determine the particle displacements in time interval of successive images and then velocity field and flow field are visualized. Two successive images are divided into small area called interrogation area and searching area as shown in Fig. 1. The peak position of the cross-correlation function is proportional to the displacement of particles, and then the velocity in the interrogation area is calculated. These transforms and calculations are repeated
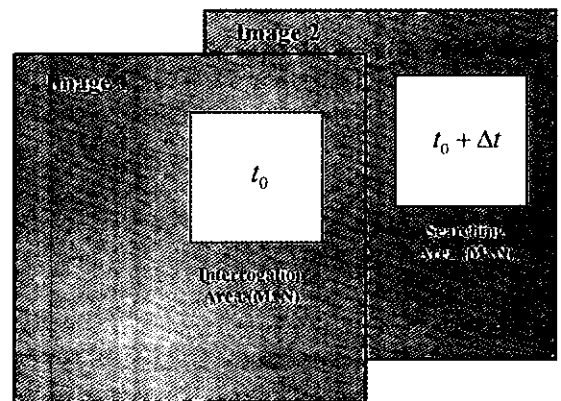

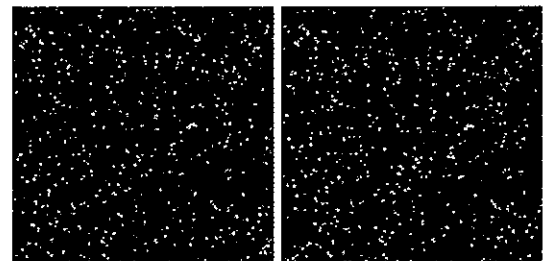**Fig. 1.** Interrogation and searching areas.

Fig. 2. 2D wall shear flow image from the Visualization Society of Japan's web site.

Fig. 3. Instantaneous velocity distributions from two successive images shown in Fig. 2.
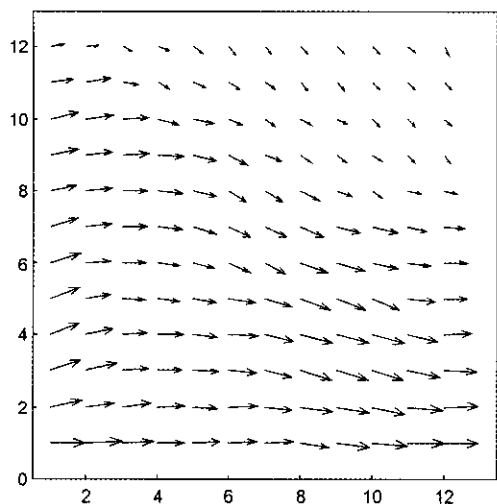

Fig. 5. Instantaneous velocity distributions from two successive images shown in Fig. 4.

to cover the whole flow field. The cross correlation PIV assumes the velocity to be relatively uniform within a search region and no change in the flow pattern between two successive images.

To examine the developed PIV system, we use 2D wall shear flow images of 256×256 pixels as shown in Fig. 2. Those were provided by the Visualization Society of Japan's PIV-Standard Project (http//www.vsj.or.jp/piv/image-e.html). The resulting velocity vectors are plotted in Fig. 3 showing satisfactory ones, in which the AOI of 64 pixel is used. The image shown in Fig. 4 is an example of images taken in 0.15 sec interval from PIV under wave condition of period 1.96 sec, wave height 2.38 cm and water depth 25 cm and the resulting velocity vectors are plotted in Fig. 5. The threshold level used for image is 20
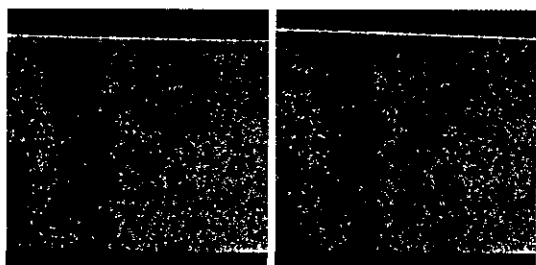
and the AOI used here is of 128 pixels.

2. PIV EXPERIMENTS

Former experimental works were focused on the measurement of the water surface displacements without taking the flow patterns around the submerged obstacle into account. Although it was expected that such a obstacle permits sea water exchange between offshore and inner harbour water bodies, it was not only measured but also predicted how much water mass could be circulated, particularly in the case of breaking waves. This fact led to the idea to visualize the flow field around the plate to derive detailed information about the flow distributions.

The submerged plate breakwater was set in a Sungkyunkwan University wave flume that consisted of a wave generator, a submerged plate model, and beach zones. The flume is 10 m long, 0.4 m wide and 0.5 m deep with the still water depth being maintained at 0.25 m. The regular waves are generated by a piston-type wave paddle. The bottom and side walls of the flume are glass to allow easy optical access. At the far end of the flume, there is an absorbing beach zone which disperses the remaining wave energy and limits reflections. The length and thickness of a plate are 1m and 1cm, respec-

Fig. 4. Two successive images taken in 0.15 sec interval (wave condition: wave height=2.38 sec, wave period=1.96 sec, water depth=25 cm).
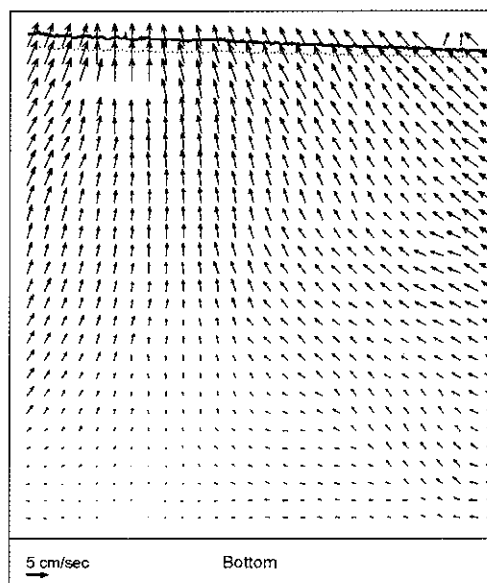
tively and the depth from plate to bottom is 16.5 cm.

As shown in Fig. 6, three resistance type wave gages were used to make simultaneous wave profile measurements; the first gage was at 1.25 m upstream of a plate center, the second at 1.25 m downstream, and the third gage was mounted on a moving cart. The cart measured from 2.5 m upstream to 1.25 m downstream of a plate center. Wave gages were connected with amplifier
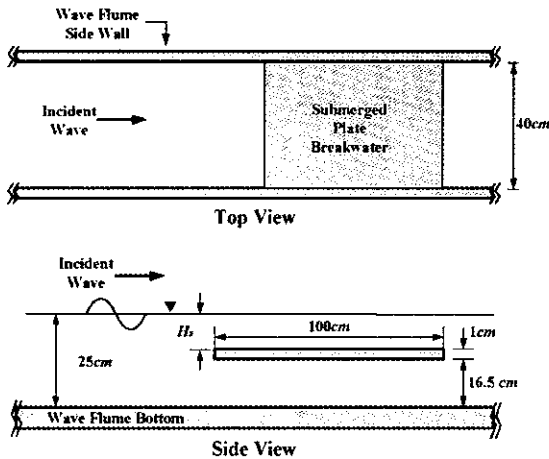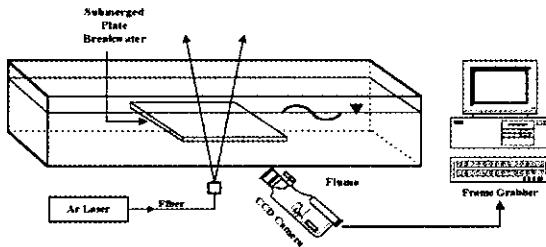

Fig. 6. Positions of wave gages and a submerged plate breakwater.

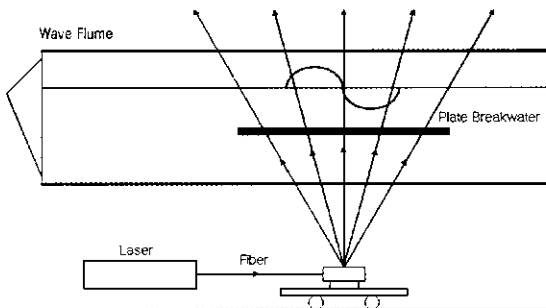**Fig. 7.** Experimental apparatus for a PIV measurement system.

Fig. 8. Schematic diagram of laser projection.

increasing analog signal. Then the DaqBoard 100A (Daq-Board), A/D converter, changes a conditioned signal into a corresponding digital number. And the digital numbers are saved as ascii format.

A schematic description of the PIV experiment setup is shown in Fig. 7, which consists of the laser pulse source and image capturing system. The fluid velocity was obtained using optical and digital processing techniques. A laser system consisting of Spectra-Physics Argon ion laser (Model 2020 Ion Laser) was used to provide the continuous beam, as shown in Fig. 8. Pulse produced by the laser has a pulse width of 6 mm. The pine pollens were used as seeding particles. The displacement fields were recorded by SMD-1M60 CCD camera (Silicon Mountain Design) mounted a 50 mm Nikkor lens (Nikon). The data were stored digitally using an AM-MTD (Imaging Technology) frame grabber and recorded with the spatial resolution of 1024×1024 or 512×512 pixels gray-level images from the CCD camera. To extract velocity distributions from the successive images, Matlab by the Math Works, a manipulation software package, was used to process the images on the 586 PC. In this experiment, 512×512 resolution were recorded and the interrogation area of 64×64 pixel was used.

3. RESULTS

3.1 Discharging Rate of Return Flow

A secondary effect of overtopped surface waves is the creation of fluid motions that is effective in the sea water exchange. Averaging over one wave period, continuity of mass must be satisfied at every cross section; shoreward flow at the upper layer (over a plate) and return flow at the lower layer (under a plate) as shown in Fig. 9. The flow field under a plate as shown in Fig. 10 was investigated to estimate the rate of wave-induced mean flow circulating
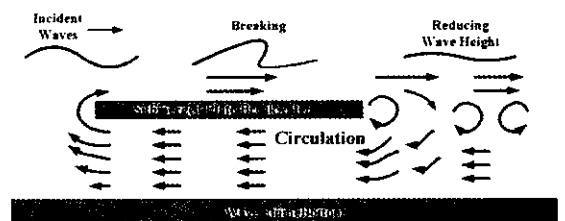

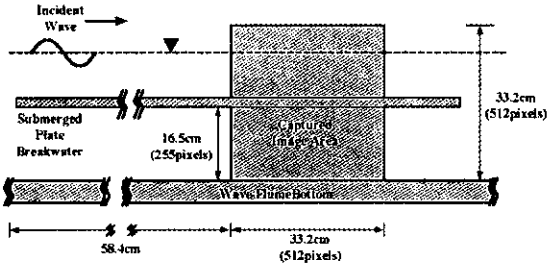**Fig. 9.** Circulationg flow around a plate breakwate.

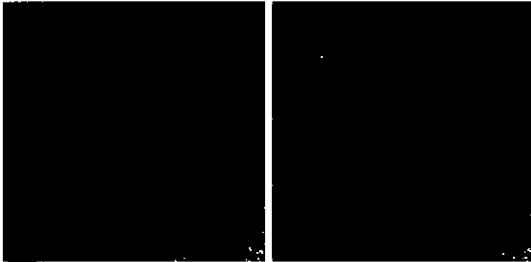**Fig. 10.** Image-captured zone for measurement of return flow.

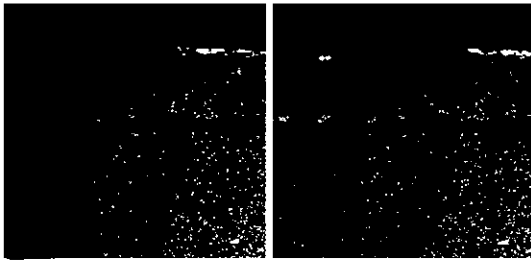**Fig. 11.** Two successive raw images taken in 0.033s ec interval (H=5.6 cm, T=1 sec).

Fig. 12. Thresholded images of two raw images shown in Fig. 10.

Fig. 13. Instantaneous velocity vectors resulted from two thresholded images shown in Fig. 11.

Table 1. Experimental wave conditions and resulting wave-averaged velocities

Wave Period (sec)	Incident Wave Height (cm)	Wave-Averaged Velocity (cm/sec)	Figure Number
0.8	4.1	5.99	Fig. 14
	9.5	12.62	Fig. 15
1.0	3.0	0.9	Fig. 16
	7.6	7.68	Fig. 17

around a plate because it is easier to measure than the surface wavy flow. The scanned area corresponds to a square region with the absolute length of 33.2 cm on a side. Distance from a head of plate to left boundary of scanned area was 60 cm.

First, an example of an instantaneous velocity field for the wave condition of period 1.0 sec is presented: Fig. 11 shows two successive images taken in interval 0.0359 seconds by CCD camera and Fig. 12 shows thresholded images. The resulting instantaneous velocity vectors are shown in Fig. 13. The shutter speed of CCD camera has been proven to be somewhat slow in tracking particles at the upper layer with strong turbulent intensity. That is, the particle images form scratched lines to yield erroneous
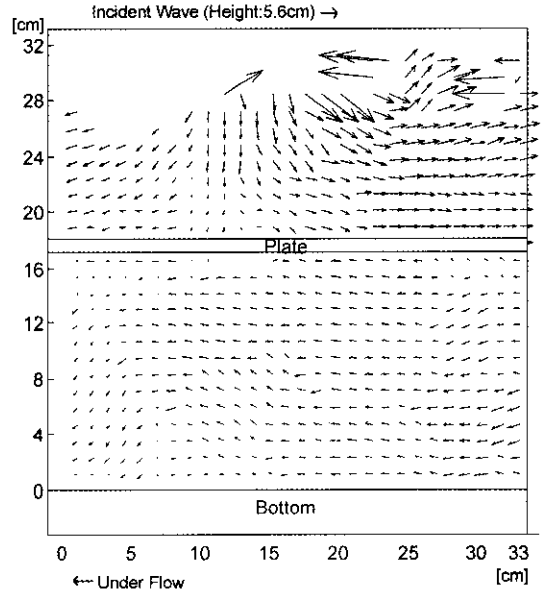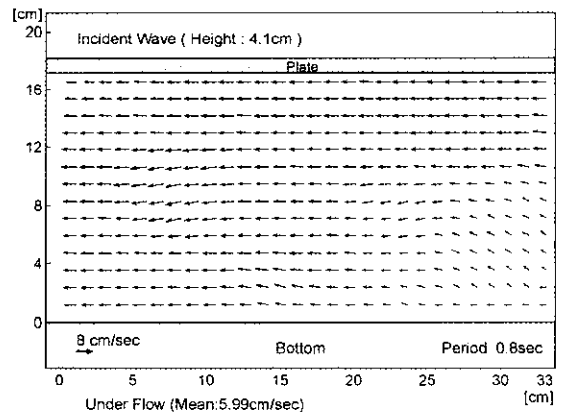

Fig. 14. Wave-averaged velocity vectors under a plate (T=0.8 sec, H_i=4 cm).
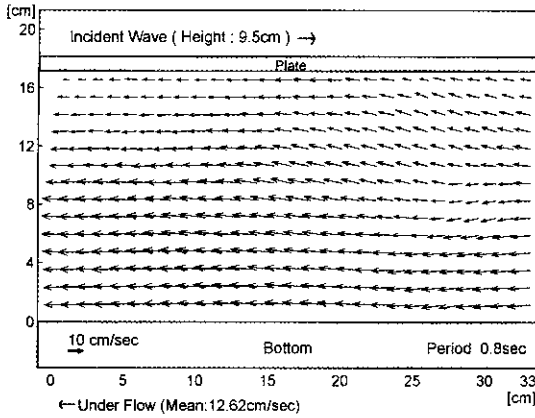
Fig. 15. Wave-averaged velocity vectors under a plate (T=0.8 sec, H_i=9.5 cm).
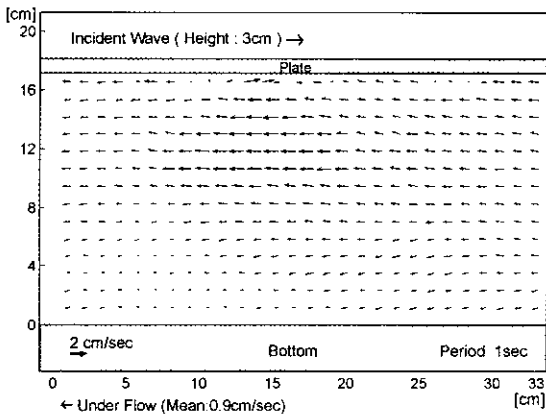

Fig. 16. Wave-averaged velocity vectors under a plate (T=1.0 sec, H_i=3.0 cm).
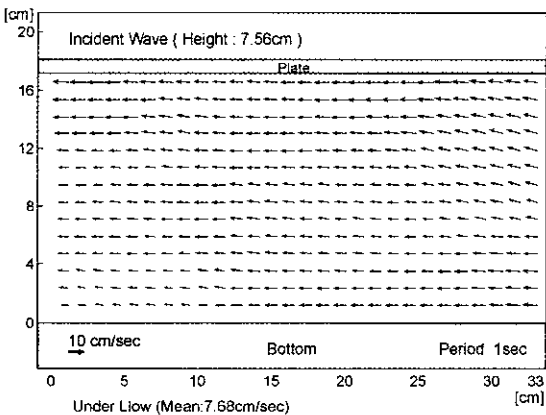

Fig. 17. Wave-averaged velocity vectors under a plate (T=1.0 sec, H_i=7.6 cm).

vectors. To solve this problem, the synchronized choking system is required between CCD camera and lighting source in order to catch the shortly exposed image. The bubbles formed with wave breaking distort the perceived location of particles so as to make serious problem in tracking a particle.

Figs. 14~17 show the return flows under a plate which were averaged over a period. Differently from the strong wavy motion over a plate, nearly parallel flow was observed under a plate. The incident wave conditions and resulting wave-averaged velocities are presented in Table 1.

The measured rates of return flow appeared to be nearly proportional to the square of incident wave height. Therefore, as shown in Fig. 18, the measured rates of return flow could be compared with values of return flow in surf zone model. The return flow in surf zone model is estimated by the volume flux ($=E/\rho C$), in which the incident volume flux is assumed to be all transmitted over a plate:

$$\bar{u} = \frac{1}{(d-d_s)\rho C_i} \frac{E_i}{} = \frac{g}{8(d-d_s)} \frac{H_i^2}{C_i} \tag{1}$$

where d is the the water depth, d_s the depth over a plate, ρ the water density, C_i the incident wave celerity, E_i the incident wave energy, and H_i the incident wave height. The fact that mean velocity follows the curve given by Eq. (1) may prove that nonlinear property related wave-induced mass flux is mainly driven from crest to trough level of waves as described by Phillips (1969).
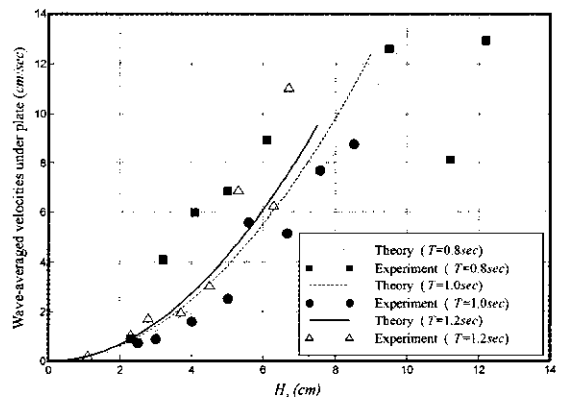

Fig. 18. Measured flow rates vs. estimated flow rates by the linear wave theory.

3.2 Flow Pattern in the Onshore Side

The submerged breakwater permits wave overtopping and the overtopping waves generate a strong rotational velocity field in the onshore region of the plate breakwater. The wave overtopping process may transmit significant wave energy toward the harbour zone which the breakwater is supposed to protect. The experimental study for the bottom-seated, submerged breakwater by Lee, Zhuang and Chang (1993) showed that wave overtopping induces strong vortices and large water particle velocities in the shoreward region behind the breakwater and a jet-like water mass induced by overtopping waves are capable of removing the armor units of breakwater and scouring the bed in the shoreward region of the breakwater. However, the rotational flow for the plate type might be reduced as the lower water body absorbs the energy like the sponge. In order to investigate such rotational flow in detail, the developed PIV system was also installed in the plane of the down-wave edge as shown in Fig. 19. The scanned area corresponds to a square region of 33.2×33.2 cm. Toe of captured image area is located at 5.74 cm seaward from the rear edge of a plate. The two experimental studies of
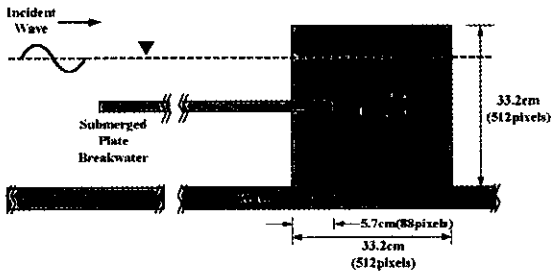
Fig. 19. Image-captured zone on the onshore side.

Table 2. List of presented figures

Subjects	Case A	Case B
	T=0.8 sec	T=1.0 sec
	H_i=2.3 cm	H_i=2.5 cm
Wave-averaged currents	Figure 20	Figure 21
Wave-averaged divegence contours	Figure 22	Figure 23
Flow balances	Figure 24	Figure 25
Wave-averaged vorticity contours	Figure 26	Figure 27
First-order wave ellipses	Figure 28	Figure 29
Second-order wave ellipses	Figure 30	Figure 31
Wave profiles	Figure 32	Figure 33

Cases A and B were accomplished: Case A; $T = 0.8$ sec and $H_i = 2.3$ cm, and Case B; $T = 1.0$ sec and $H_i = 2.5$ cm.

The raw velocity data measured by the PIV system were analyzed using the harmonic analysis so as to obtain the mean currents, primary wave orbital motion and non-linear wave-induced motion components.
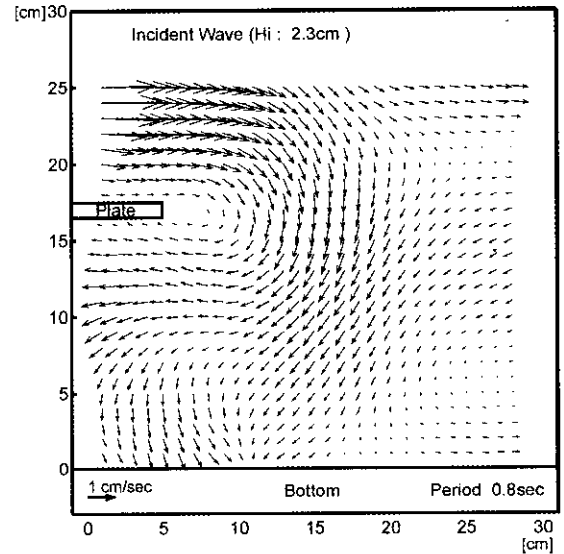
Fig. 20. Wave-averaged velocity vectors of Case A (T=0.8 sec and H_i=2.3 cm).
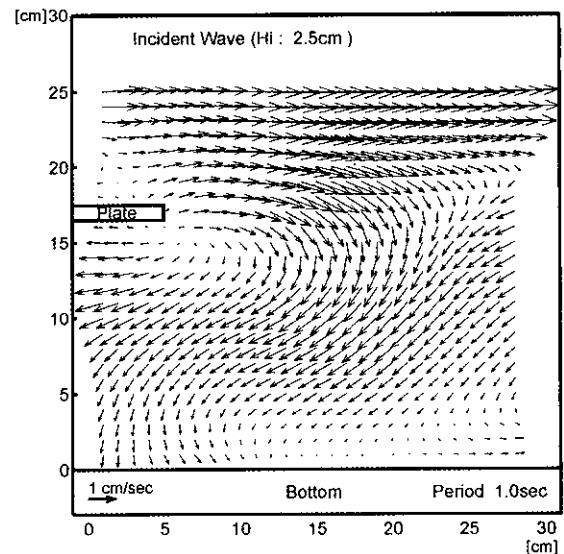
Fig. 21. Wave-averaged velocity vectors of Case B (T=1.0 sec and H_i=2.5 cm).

Wave-averaged velocity distributions obtained by PIV are shown in Figs. 20 and 21. As shown in the figure, a flow reversal manifests itself at the plane of down-wave edge. A jet-like flow is generated in upper layer and subsequent large-scale turbulent structures are evident at the shoreward plane of a plate. Within these regions, the tur-

bulence induced by the jet flow is overturning and causing strong mixing. Such jet flow supplies fresh waters into the inner bay and makes contaminated inner waters discharge out of a bay through the underway of a plate. As incident wave heights increase, the residual currents become stronger and more extend their influence shoreward.

The PIV data could be imbedded with errors. For the quantitative measures on how well the mean currents satisfied the continuity equation, the following normalized value was computed on each node.

$$\alpha = \frac{|\partial u/\partial x + \partial v/\partial y|}{|\partial u/\partial x| + |\partial v/\partial y|} \tag{2}$$

In the computation, the partial derivatives were approximated by their finite differences. This expression provides α between 0, when the continuity equation is satisfied exactly, and unity, when velocity components are independent, random variables. In incompressible flow, the flow divergence has to be zero, but the calculated divergences are far from the zero as shown in Figs. 22 and 23. Errors are significant in the reversal zone of flow. Zhang et al. (1997) showed that the deviation from the continuity equation could decrease rapidly with increasing control volume. Other reasons of such the deviation might be non-uniform distribution of particles and out-of-plane motion as well as the falling motion of paricles.
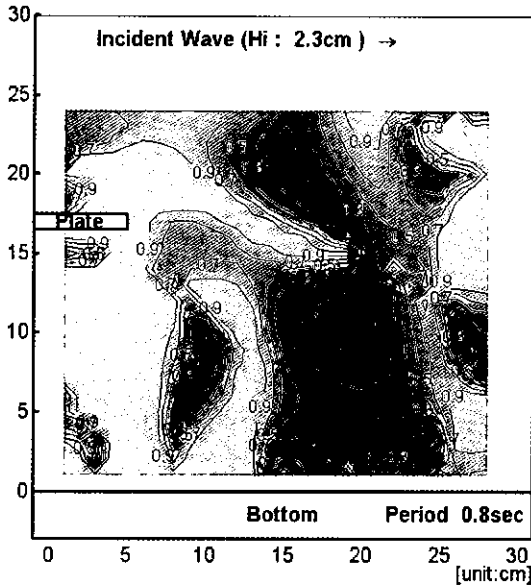

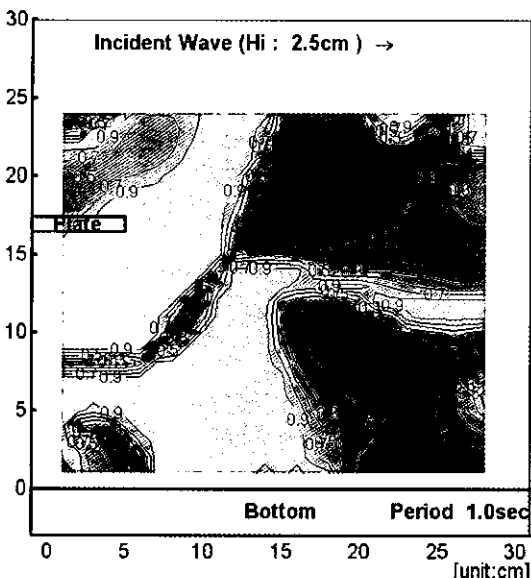**Fig. 22.** Normalized divergence of Case A (T=0.8 sec and H_i=2.3 cm).

Fig. 23. Normalized divergence of Case B (T=1.0 sec and H_i=2.5 cm).
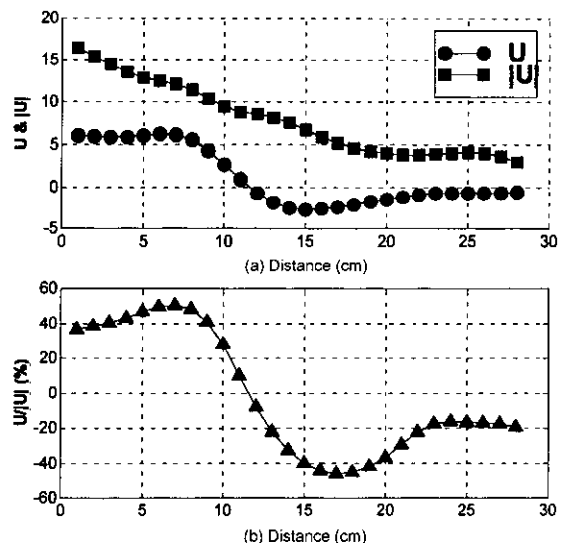

Fig. 24. Flow balance of horizontal components of Case A (T=0.8 sec and H_i=2.3 cm).
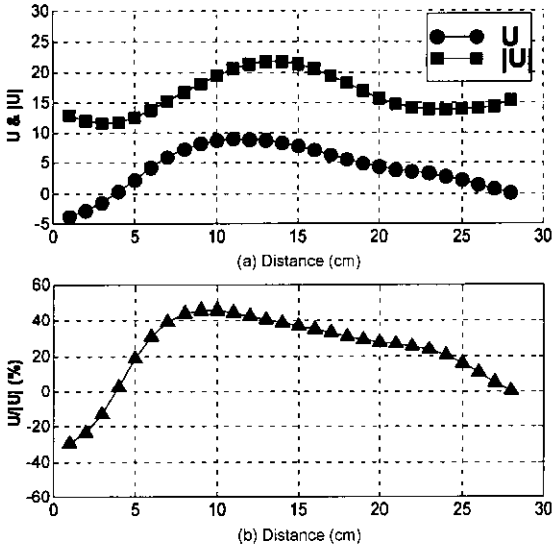
Fig. 25. Flow balance of horizontal components of Case B (T=1.0 sec and H_i=2.5 cm).

After steady state attained, the depth-integrated values of horizontal component of velocity vectors, U, also have to be zero to satisfy the mass conservation rule:

$$U = \int_{-h}^{0} u\,dz \cong \sum_{j=1}^{J} u_j \Delta z \qquad (3)$$

where J is the total index in z-direction. Downstream of the plate, the depth-integrated values of absolute horizontal components of velocity vectors, $|U|$, show the trend of decreasing due to the flow reversal:

$$|U| = \int_{-h}^{0} |u|\,dz \cong \sum_{j=1}^{J} |u_j| \Delta z \qquad (4)$$

The U and $|U|$ are plotted in Figs. 24(a) and 25(a). As similar as the divergence test, however, the U values indicate the violation of mass conservation rule. The earlier flow reversal is found in Case A which has lower incident wave height than Case B. In order to examine if the error is significant or not, the quantity of U normalized by $|U|$, U', is also plotted in Figs. 24(b) and 25(b).

$$U' = \frac{\int_{-h}^{0} u\,dz}{\int_{-h}^{0} |u|\,dz} \cong \frac{\sum_{j=1}^{J} u_j}{\sum_{j=1}^{J} |u_j|} = \frac{U}{|U|} \qquad (5)$$

Results shown in Figs. 24 and 25 convey that the flow

patterns look reasonable in general, but the vector quality does not satisfy the mass balance well enough. In Figs. 24 and 25, the circles ($\bigcirc$) indicate the depth-integrated value of horizontal velocity components. The squares ($\square$) indicate the depth-integrated value of horizontal absolute velocity components. The triangles ($\triangle$) are normalized value.

Next, this paper is concerned with vorticity strength as an alternative way of analyzing flow. Vorticity is defined as the intensity of flow rotationality and demonstrates the flow structure better than the velocity distributions shown before in some sense. We consider the vorticity on the scale of the wave crest length or wave length rather than the associate turbulent motions, such as is important in describing mean currents. In the present experiments, the vortices might be generated by three mechanisms; first is from the surface, second is by the presence of the plate, and last is by flow reversal. At the present stage, a PIV system is able to capture only the no breaking status, and then the vortices generated by the presence of a plate might be not as strong as the one by the flow reversal.

Two dimensional velocity data in a plane allow determination of only the out-of-plane component of vorticity:

$$\omega = \frac{1}{2}\left(\frac{\partial v}{\partial x} - \frac{\partial u}{\partial y}\right) \qquad (6)$$

Rather than translating Eq. (6) directly to first-order differences, ω is evaluated by computing the local circulation around a closed contour surrounding the point and invoking Stokes' theorem to relate the circulation per unit area to the vorticity:

$$\omega = \lim_{A \to 0} \frac{\Gamma}{A} \qquad (7)$$

The numerical approximation to Eq. (6) is implemented with a closed contour defined by the eight points surrounding the node at which the vorticity is to be evaluated as

$$\omega = \frac{\Delta l}{4\Delta x \Delta y} \times \left\{ \begin{array}{l} u_{(i,j-1)} + \frac{1}{2}(u_{(i+1,j-1)} + v_{(i+1,j-1)}) \\[6pt] u_{(i,j+1)} - \frac{1}{2}(u_{(i-1,j+1)} + v_{(i-1,j+1)}) \end{array} \right.$$
$$\left. \begin{array}{l} + v_{(i+1,j)} - \frac{1}{2}(u_{(i+1,j+1)} + v_{(i+1,j+1)}) - \\[6pt] - v_{(i-1,j)} - \frac{1}{2}(u_{(i-1,j-1)} + v_{(i-1,j-1)}) \end{array} \right\} \qquad (8)$$
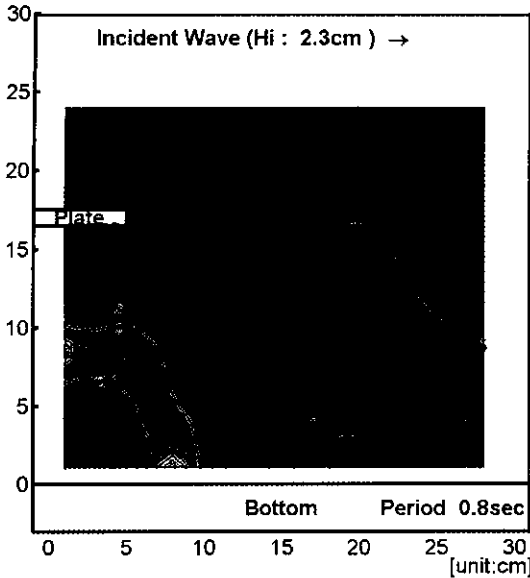
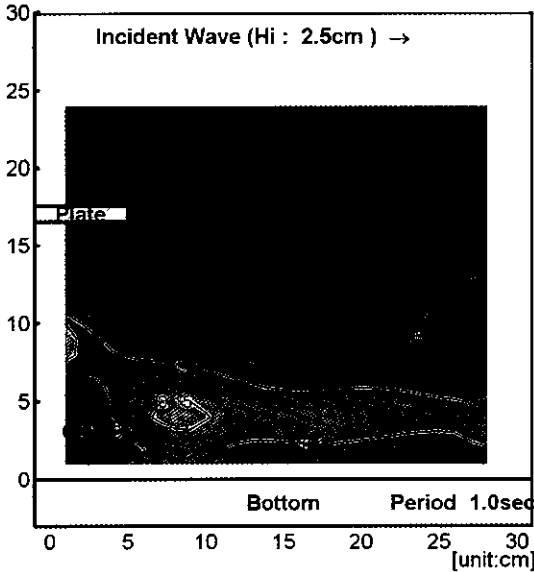**Fig. 26.** Vorticity contours of Case A (T=0.8 sec and H_i=2.3 cm).

Fig. 28. First-order wave ellipses of Case A (T=0.8 sec and H_i=2.3 cm).

Fig. 27. Vorticity contours of Case B (T=1.0 sec and H_i= 2.5 cm).

Fig. 29. First-order wave ellipses of Case B (T=1.0 sec and H_i=2.5 cm).

where Δl is the grid step size. This method was used instead of the more straightforward first-order difference scheme to provide smoothing of the vorticity field consistent with the resolution due to the PIV interrogation spot size.
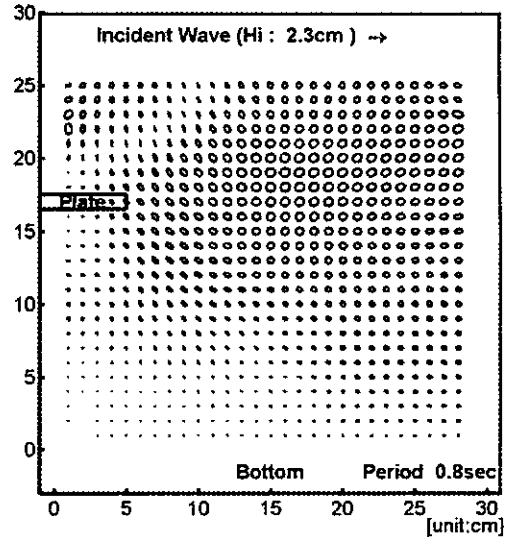
Figs. 26 and 27 show the computed vorticity contours.
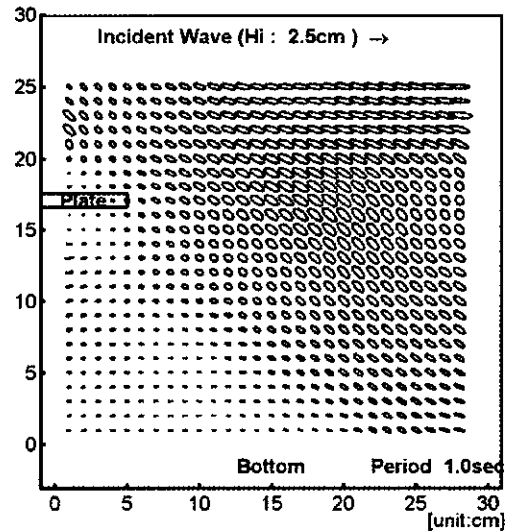
A clockwise vortex flow contains negative vorticity and a counter flow contains positive vorticity. Large clockwise vortex is found on the onshore side of the plate. However, the vortex was observed to move around in a relatively small region, and continuously changed its structure from one instant to another. The fluid being above a plate is push into inner bay side. Thus, the vortex obtains a continuous supply of energy from the separated flow while the energy of the vortex is dissipated by viscous friction.

According to this process, the formation of the clockwise vortex seems to be retained anyhow.

The overtopped waves also transmit the significant wave energy in the shoreward region with oscillatory wave trains. The motions of transmitted waves are presented by the ellipses, which are used as a graphic tool to express all instantaneous wave motion per a cycle in comprehensive manner, providing the major direction and
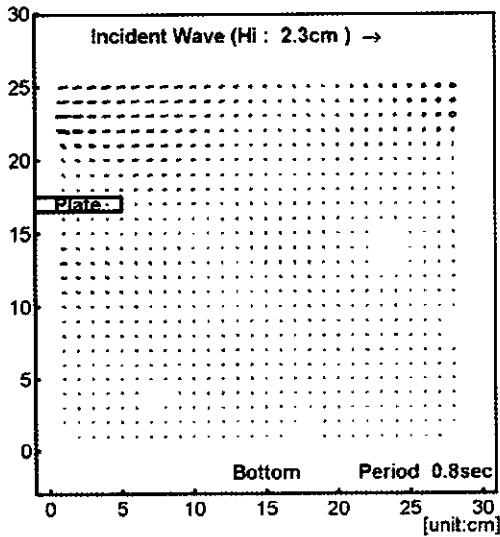

Fig. 30. Second-order wave ellipses of Case A (T=0.8 sec and H_i=2.3 cm).
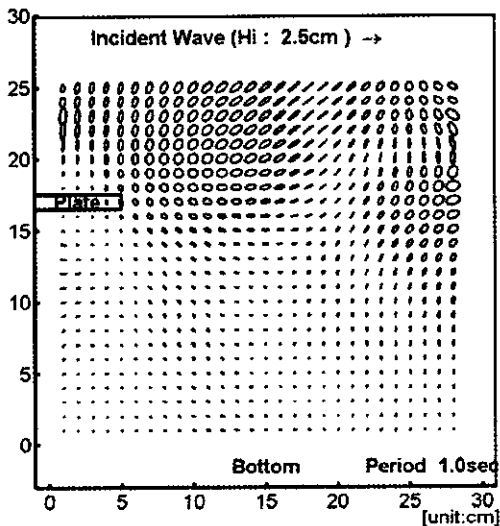

Fig. 31. Second-order wave ellipses of Case B (T=1.0 sec and H_i=2.5 cm).

magnitude of wave motions. The temporal profile of horizontal and vertical velocity components at each point was transformed into a Fourier series. Then first and second components like tidal ellipses are obtained.

The first-order wave motions are shown in Figs. 28 and 29. For T=0.8 sec, the first-order motions seem to be regular circles near the surface. The fundamental harmonic components tend to decay toward onshore side of the plate because of the recovery of water depth and the wave energy dissipation. The major motions lean to bottom at the down-wave edge and horizontally move at the bottom. For T=1.0 sec, the first-order wave motions seem to be elliptic shape all over the region and directions of motions also lean to the lower-right corner.

When the waves passing over a submerged bar or a submerged shelf with a finite width, higher harmonic components are generated due to nonlinear effect and waves are
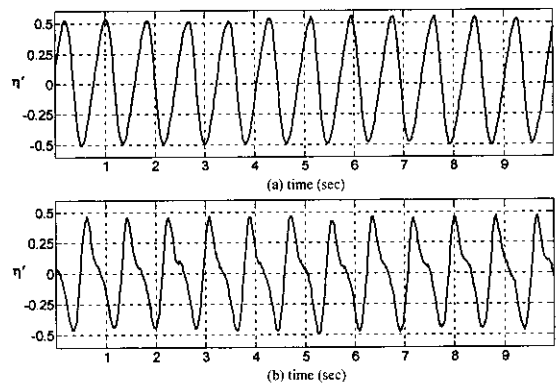

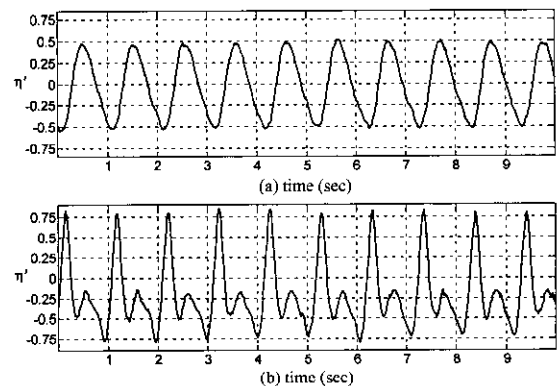**Fig. 32.** Normalized wave profile of Case A (T=0.8 sec and H_i=2.3 cm).

Fig. 33. Normalized wave profile of Case B (T=1.0 sec and H_i=2.5 cm).

generally broken and decomposed. This phenomenon is related to variation of the wave spectrum during passage over a submerged obstacle. The second-order wave ellipses are shown in Figs. 30 and 31. The second-order harmonic components are highly concentrated right after a plate edge rather than near the surface. For T=0.8 sec,
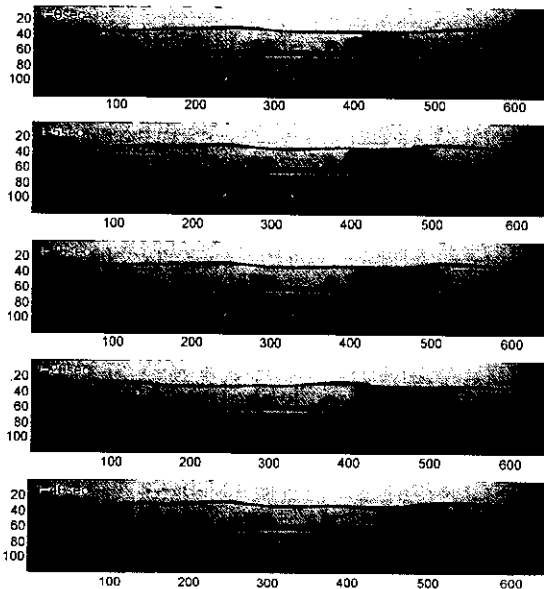

Fig. 34. Behavior of a dye cloud for Case C (T=0.8 sec and H_i=2.3 cm).
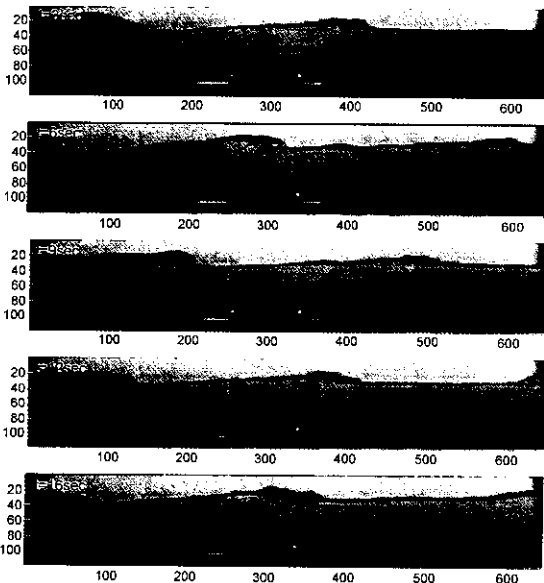

Fig. 35. Behavior of a dye cloud for Case D (T=0.8 sec and H_i=6.1 cm).

the magnitudes are not significant except the vicinity of mean surface. As shown in Fig. 31, however, the second-order ellipses become prominent for T=1.0 sec, showing high concentration right after a plate edge rather than near the surface.

In order to measure the decomposition phenomena of wave profiles due to nonlinearity, two wave gages were set; one is located at 1 m offshore from the up-wave edge, and the other is located at 1 m onshore from the down-wave edge. Wave profiles normalized by incident wave heights are given in Figs. 32 and 33, where it is confirmed that the wave nonlinearity for T=1.0 sec is more significant than that of T=0.8 sec.

4. DYE STUDY

Dye studies were conducted for visualizing a circulation pattern around a plate, identifying dispersion patterns in a mixing zone. The Rhodamine B was released into the flow right over the down-wave edge. These experimental studies were accomplished for two wave conditions: Case C; T=0.8 sec and H_i=2.3 cm (the same as Case A given in Section 3.2) and Case D; T=0.8 sec and H_i=6.1 cm (waves breaking over a plate). The movement of the dye clouds was recorded using a digital video camera and some of images are shown in Figs. 34 to 35. The video records were obtained on a large monitor to recognize the whole circulating pattern of the dye clouds.

The mixing is primarily a result of ambient turbulence naturally present in the receiving water. Therefore, the strength of mixing depends on that of the incoming flow; in other words, on the square of the incident wave height as a result in the previous section. Fig. 34 shows the behavior of dye clouds injected over a down-wave edge for the mild incident wave energy. At the onshore side of a plate, the dye cloud collapses to the bottom and splits into both ways. Such behavior of dye cloud indicates the presence of the two large-scale coherence structures which form the counter-rotating vortex pair.

For higher wave height as shown in Fig. 35, the jet-like flow over a down-wave edge is more expansively mixing with ambient fluid and the dilution occurs stronger. The extended eddy groups are diffusing dyed fluid from the center regions of the dye cloud outwards and in doing so large quantities of ambient fluid are drawn in the center

regions of the dye cloud. In reality, this mixing process occurs between the sea water and polluted inner water. Subsequently, large quantity of polluted inner water can be discharged to outer sea through the underway of a plate.

5. CONCLUSION

The wave-averaged flow pattern around a submerged horizontal plate has been examined experimentally by using a PIV system. It was found that circulating flow formed around a plate was caused by the volume flux generated as progressive waves passing over the plate. Mean currents and wave ellipses were extracted from raw velocity data by using the harmonic analysis. Dye studies were also conducted for visualizing a circulation pattern around a plate, identifying dispersion patterns in a mixing zone.

Through the experiments, it has been found that the submerged horizontal plate-type breakwater has the structural characteristic that excels the sea water exchange. The flow structure around a plate appeared to be similar to that of surf zone and the flowrate was observed to be proportional to the square of incident wave height as the same as estimated in the flow structure of the surf zone.

PIV experiments at the down-wave edge plane showed that a jet-like residual flow was generated in the upper layer of a plate and the flow collapsed at some distance causing the large-scale counter-rotating vortex pair. The turbulent intensity was also observed to be extremely high in the plane of the down-wave edge. Due to the strong mixing process, the submerged plate can be effective for water quality purification, producing a circulating flow with strong turbulence formed near the down-wave edge. For more detailed analysis of the breaking-induced flow, the studies on air-water mixing are also necessary.

ACKNOWLEDGMENT

REFERENCES

Adrian, R.J., 1991. Particle-imaging techinques for experimental fluid mechanics, *Annu. Rev. Fluid Mech.*, Vol. 23, pp. 261-304.

Aoyama T., Izumiya T., Isobe M., and Watanabe A., 1988. A study on wave control by a submerged plate, *Proc. 35th Int. Conf. Coastal Engrg.*, pp.507-511 (in Japanese).

Emarat, N., Christensen, E.D., and Forehand, D.I.M., 2000. A study of plunging breaker mechanics by PIV measurements and a Navier-Stokes solver, *Proc. 27th Int. Conf. Coast. Engrg.*, ASCE, Sydney, Australia.

Greated, C.A., Skyner, D.J., and Bruce, T., 1992. Particle image velocimetry (PIV) in the castal engineering laboratory, *Proc. 23th Int. Conf. Coast. Engrg.*, ASCE, Venice, Italy, pp. 212-225.

Iwata, K., Kawasaki, K., and Kim, D-S, 1996. Breaking limit, breaking and post-breaking wave deformation due to submerged structures, *Proc. 25th Int. Conf. Coast. Engrg.*, ASCE, Orlando, Florida, pp. 2338-2351.

Kimura, I., and Takamori, T. 1986. Image processing of flow around a circular cylinder by using correlation technique, *Flow Visualization*, Vol. 4, pp. 221-226.

Lee, J.J., Zhuang, F., and Chang, C., 1993. Kinematics of wave overtopping on marine structure, *Proc. 2nd Int. Symp. Ocean Wave Meas. & Anal.*, New Orleans, Louisiana. pp. 821-834.

Murakami, H., Itoh, S., Hosoi, Y., and Sawamura, Y., 1994. Wave induced flow around submerged sloping plates, *Proc. 24th Int. Conf. Coast. Engrg.*, ASCE, Kobe, Japan, pp. 1700-1712.

Petti, M., Quinn, P.A., Liberatore, G., and Easson, W., 1994. Wave velocity field measurements over a submerged breakwater, *Proc. 24th Int. Conf. Coast. Engrg.*, ASCE, Kobe, Japan, pp. 525-539.

Phillips, O.M., 1969. The dynamics of the upper ocean, *Cambridge University Press*, Cambridge.

Quinn, P.A., Skyner, D.J., Gray, C., Greated, C.A., and Easson, W.J., 1993. Critical analysis of the particle image velocimetry technique as applied to water waves, *In Flow Visualization and Image Analysis*, Ed. F.T.M. Nieuwstadt, Kluwer Academic Publishers, Dordrecht, The Netherlands.

Yamada, F., and Takikawa, K., 2000. Determination of internal characteristics of breaker deformation, *Abstracts of Proc. 27th Int. Conf. Coast. Engrg.*, ASCE, Sydney, Australia.

Yu, X., Isobe, M. and Watanabe, A., 1991. Wave force on submerged plate, *Proc. 38th Conf. On Coastal Engrg.*, pp. 671-675 (in Japanese).

Zhang, J., Tao, B., and Katz, J., 1997. Turbulent flow measurement in a square duct with hybrid holographic PIV, *Experiments in Fluid*, Vol. 23, pp. 373-381.